



Title	Quantum cascade laser absorption spectroscopy with the amplitude-to-time conversion technique for atmospheric-pressure plasmas
Author(s)	Yumii, Takayoshi; Kimura, Noriaki; Hamaguchi, Satoshi
Citation	Journal of Applied Physics. 2013, 113(21), p. 213101
Version Type	VoR
URL	<a href="https://hdl.handle.net/11094/78468">https://hdl.handle.net/11094/78468</a>
rights	This article may be downloaded for personal use only. Any other use requires prior permission of the author and AIP Publishing. This article appeared in Journal of Applied Physics 113, 213101 (2013) and may be found at <a href="https://doi.org/10.1063/1.4808261">https://doi.org/10.1063/1.4808261</a> .
Note	

*The University of Osaka Institutional Knowledge Archive : OUKA*

<https://ir.library.osaka-u.ac.jp/>

The University of Osaka

# Quantum cascade laser absorption spectroscopy with the amplitude-to-time conversion technique for atmospheric-pressure plasmas

Cite as: J. Appl. Phys. **113**, 213101 (2013); <https://doi.org/10.1063/1.4808261>

Submitted: 07 March 2013 . Accepted: 15 May 2013 . Published Online: 03 June 2013

Takayoshi Yumii, Noriaki Kimura, and Satoshi Hamaguchi



View Online



Export Citation



CrossMark

## ARTICLES YOU MAY BE INTERESTED IN

[Raman spectroscopy of piezoelectrics](#)

Journal of Applied Physics **113**, 211301 (2013); <https://doi.org/10.1063/1.4803740>



## Your Qubits. Measured.

Meet the next generation of quantum analyzers

- Readout for up to 64 qubits
- Operation at up to 8.5 GHz, mixer-calibration-free
- Signal optimization with minimal latency

Find out more



# Quantum cascade laser absorption spectroscopy with the amplitude-to-time conversion technique for atmospheric-pressure plasmas

Takayoshi Yumii,<sup>1,2,a)</sup> Noriaki Kimura,<sup>1,2</sup> and Satoshi Hamaguchi<sup>2</sup>

<sup>1</sup>Mitsui Engineering and Shipbuilding Co., Ltd., Tamahara 3-16-1, Tamano, Okayama 706-0014, Japan

<sup>2</sup>Graduate School of Engineering, Osaka University, Yamadaoka 2-1, Suita, Osaka 565-0871, Japan

(Received 7 March 2013; accepted 15 May 2013; published online 3 June 2013)

The NO<sub>2</sub> concentration, i.e., density, in a small plasma of a nitrogen oxide (NO<sub>x</sub>) treatment reactor has been measured by highly sensitive laser absorption spectroscopy. The absorption spectroscopy uses a single path of a quantum cascade laser beam passing through a plasma whose dimension is about 1 cm. The high sensitivity of spectroscopy is achieved by the amplitude-to-time conversion technique. Although the plasma reactor is designed to convert NO in the input gas to NO<sub>2</sub>, it has been demonstrated by this highly sensitive absorption spectroscopy that NO<sub>2</sub> in a simulated exhaust gas that enters the reactor is decomposed by the plasma first and then NO<sub>2</sub> is formed again, possibly more than it was decomposed, through a series of gas-phase reactions by the time the gas exits the reactor. The observation is consistent with that of an earlier study on NO decomposition by the same type of a plasma reactor [T. Yumii *et al.*, J. Phys. D **46**, 135202 (2013)], in which a high concentration of NO<sub>2</sub> was observed at the exit of the reactor. © 2013 AIP Publishing LLC. [<http://dx.doi.org/10.1063/1.4808261>]

## I. INTRODUCTION

Nitrogen oxide (NO<sub>x</sub>) emitted from combustion systems such as diesel engines and boilers can adversely affect our environments, causing air pollution and acid rain. Reduction of NO<sub>x</sub> emission from such systems is therefore vital for maintaining healthy environments. Typical NO<sub>x</sub> reduction technology relies on catalytic reactions.<sup>1–3</sup> Under certain conditions of NO<sub>x</sub> emission (typically with a relatively high concentration of oxygen), however, the operating temperature of the catalyst system needs to be high,<sup>4,5</sup> which reduces energy efficiency for the catalytic reactions. NO<sub>2</sub> can be efficiently converted to N<sub>2</sub> and O<sub>2</sub> or other harmless gases by catalysts such as  $\gamma$ -alumina<sup>6</sup> or reducing agents such as Na<sub>2</sub>SO<sub>3</sub>.<sup>7</sup> Only NO can be decomposed directly by catalysts that are currently available. Therefore many efforts have been focused on developing plasma treatment systems that can oxidize NO to NO<sub>2</sub>.<sup>8–10</sup>

To use a plasma for typical exhaust gas treatment, it must be generated at atmospheric pressure. Examples of non-thermal plasmas, which are typically more energy efficient than thermal plasmas for gas treatment, include corona discharges<sup>11,12</sup> and dielectric barrier discharges.<sup>13,14</sup> Most non-thermal atmospheric pressure plasmas require high voltage pulsed or AC power for plasma generation. Recently Yumii *et al.*<sup>15</sup> have proposed a radio-frequency (RF) resonant plasma reactor, which can be operated by low-voltage RF power and generate a plasma by high voltage formed by electromagnetic resonance inside the reactor.

To confirm whether specific molecular species of interest such as NO or NO<sub>2</sub> is indeed decomposed, one needs to measure its concentration in the gas mixture. Absorption spectroscopy is a well-established technique for the

measurement of gas concentrations of various atomic and molecular species. If the gaseous species of interest has a low concentration or the optical path for laser absorption is short, absorption spectroscopy is required to detect small attenuation of laser light that passes through the gas. Since typical non-thermal atmospheric-pressure plasmas are small in size and the concentrations of gaseous species that we are interested in for gas treatment are typically at the ppm levels, absorption spectroscopy of our interest is required to have high sensitivity.

In this study, we use a highly sensitive absorption spectroscopy based on a quantum cascade laser (QCL)<sup>16–19</sup> and the amplitude-to-time conversion (ATTC) technique.<sup>20</sup> A QCL is a semiconductor laser with relatively high beam intensity. The wavelength of a QCL depends on its multi-layered structures of semiconductor materials so that a QCL could be designed and manufactured to emit a laser beam with a specific wavelength that one desires (typically within the range from 3  $\mu$ m to 100  $\mu$ m). Especially QCLs with wavelengths corresponding to well-known molecular absorption lines are commercially available at relatively low cost.

The ATTC<sup>20</sup> refers to a technique that converts the amplitude of repeated pulsed signals with statistical noises to the average rise time of the signals. As will be explained later, the ATTC technique allows a sensitive measurement of small changes in the electrical signal representing a laser beam amplitude.

The goal of this study is to demonstrate that QCL absorption spectroscopy with the ATTC technique can be used as a diagnostic tool for the gas concentration measurement of a non-thermal atmospheric pressure plasma with a relatively short optical path length. In this work, we have measured the NO<sub>2</sub> concentration in the discharge region of a plasma reactor designed for NO<sub>x</sub> treatment and shown that NO<sub>2</sub> in a simulated exhaust gas can be decomposed by the plasma under various discharge conditions.

<sup>a)</sup>Electronic mail: yumii@ppl.eng.osaka-u.ac.jp

The rest of the paper is structured as follows. In Sec. II, the basic concept of the ATTC technique applied to laser absorption spectroscopy is briefly reviewed. In Sec. III, the experimental system including a NO<sub>x</sub> treatment plasma reactor is explained in detail. Experimental data and discussion on the results are presented in Secs. IV and V. Section VI summarizes this study and presents the conclusion.

## II. CONCEPT OF LASER ABSORPTION SPECTROSCOPY WITH THE ATTC TECHNIQUE

Figure 1 shows a conceptual diagram of laser absorption spectroscopy with an ATTC circuit. The system consists of a QCL laser, a photo detector, an amplitude-to-delay-time converter, and a waveform regenerator. Emission of a laser pulse is triggered by an external signal of a square waveform with interval time  $t$ . The laser pulse width of this system was 120 ns. Other parameters of the experiments will be given in Sec. III. The photo detector converts a detected optical pulse to an electrical signal. The amplitude-to-delay-time converter has two input terminals. One is for output signals of the photo detector, and the other is for reference voltage. The amplitude-to-delay-time converter generates a square pulse signal with a sharp rising edge only when the amplitude of the input signal becomes higher than the reference voltage. When the waveform regenerator receives an input signal from the amplitude-to-delay-time converter, it generates a pulse signal of a square waveform which has the same amplitude and width as those of the signal that triggered the laser initially. In this way, the sequence of laser emission and waveform regeneration can be repeated. We call the combination of amplitude-to-delay-time converter and waveform regenerator an ATTC.

We now explain how the ATTC works to detect small variation in the amplitude of photo detector signals. First we assume that the plasma is in steady state and therefore photo detector's output signal always has essentially the same amplitude for every laser pulse that passes through the plasma. What needs to be determined here is the difference in amplitude of the photo detector signals between the cases where the plasma is on and off. Suppose a gas that we are interested in (such as NO<sub>2</sub>) can be decomposed by the plasma. In this case, when the plasma is on, the gas is decomposed by the plasma and its concentration is lower. Therefore the laser light is absorbed less by the gas, and the photo detector

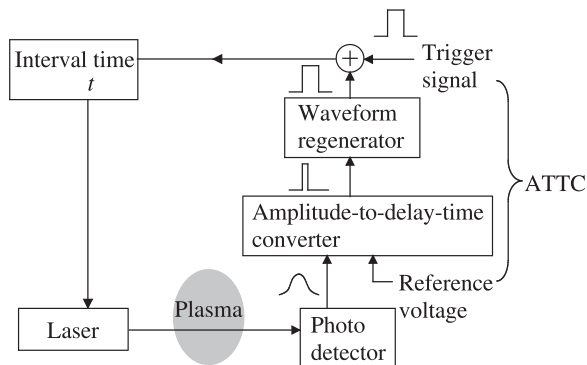


FIG. 1. Conceptual diagram of laser absorption spectroscopy with an ATTC circuit. The laser is pulsed by external trigger signals.

signal is stronger. On the other hand, when the plasma is off, the gas is more abundant and absorbs more laser light, which leads to weaker signals of the photo detector.

Figure 2 shows these two cases; (a) represents the case with larger detector signals (with no laser absorption) and (b) the case with slightly smaller detector signals (with laser absorption). The horizontal and vertical axes represent time and the signal amplitudes. Here the interval time between the trigger signal and laser emission is denoted by  $t$ , as in Figure 1. The delay time generated by the amplitude-to-delay-time converter is denoted by  $\Delta t_i$  [ $i = 1, 2$  for (a) and (b)]. Thus the time  $(t + \Delta t_i)$  represents the period for each laser shot operation.

The difference in delay time  $\Delta t$  between (a) and (b) of Figure 2 can be shown to be proportional to the laser light absorbance  $\alpha$  in the following manner. In Figure 3, the photo detector signals of Figures 2(a) and 2(b) are redrawn together, with the photo detector signal of (a) is denoted by function  $f(t)$ . The signal (b) is then denoted by  $(1 - \alpha)f(t)$ . Since the relation

$$f(\Delta t_1) = (1 - \alpha)f(\Delta t_2)$$

holds, we obtain

$$\alpha = \frac{f'(\Delta t_1)}{f(\Delta t_1)} (\Delta t_2 - \Delta t_1) \quad (1)$$

as long as  $\alpha \ll 1$ .

If the laser shot operation is repeated  $N$  times, the total time for the operation sequence is given by  $T_1 = N(t + \Delta t_1)$  for Figure 2(a), which we call the sequence time. Similarly, in (b), where the signals are smaller by  $1 - \alpha$  due to absorbance, the sequence time is given by  $T_2 = N(t + \Delta t_2)$ . The difference is  $T_2 - T_1 = N(\Delta t_2 - \Delta t_1)$ , which call the sequence time difference. As shown above, the sequence time difference is proportional to the absorbance  $\alpha$ . It should be noted that even if the difference  $\Delta t_2 - \Delta t_1$  is small, the sequence time difference  $T_2 - T_1 = N(\Delta t_2 - \Delta t_1)$  can be large if we

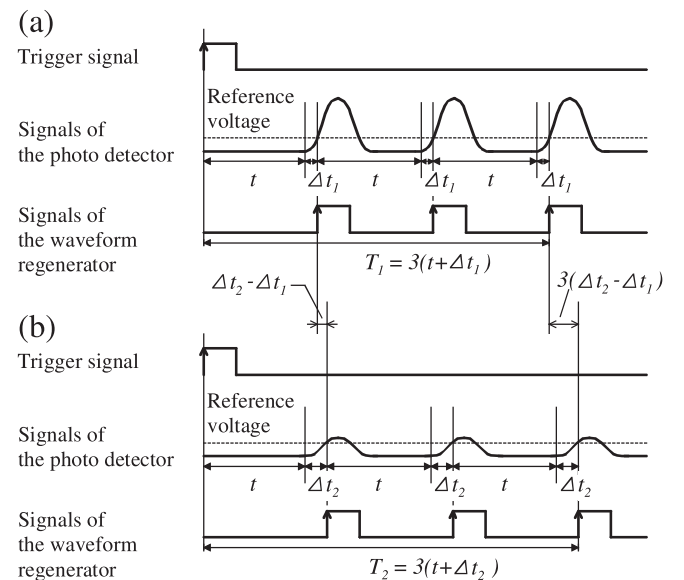


FIG. 2. Timing diagram of the circuit of Figure 1. The sequence time for  $N$  laser shot operations is longer for the signals with a smaller amplitude. Here (a) shows repeated signals with a large amplitude whereas (b) shows repeated signals with a small amplitude.

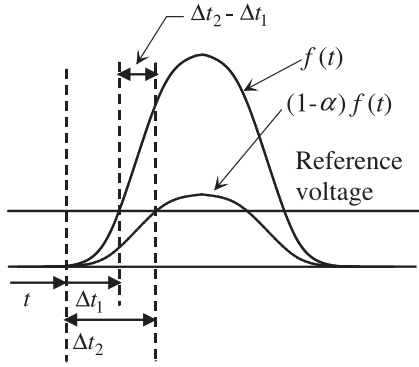


FIG. 3. Relation between the difference in delay time  $\Delta t_2 - \Delta t_1$  and absorbance  $\alpha$ . The function  $f(t)$  and  $(1-\alpha)f(t)$  represent the photo detector signals of Figures 2(a) and 2(b).

select a sufficiently large  $N$ . In addition, the signal-to-noise (S/N) ratio can typically improve in proportion to  $\sqrt{N}$ . In this way, the ATTC technique for laser absorption spectroscopy converts the absorbance  $\alpha$  to the sequence time difference  $N(\Delta t_2 - \Delta t_1)$ . The comparison between the direct measurement of difference in photo detector signals (i.e., conventional technique for laser absorption spectroscopy) and the absorbance measurement through the sequence time difference (i.e., ATTC technique) is discussed in Appendix B.

### III. EXPERIMENTAL SYSTEM OF NO<sub>2</sub> CONCENTRATION INSIDE A RESONANT PLASMA REACTOR

Figure 4 shows a block diagram of the absorption spectroscopy measurement system with a plasma reactor used in

this study. With this system, we measure the NO<sub>2</sub> concentration in the plasma reactor for NO<sub>x</sub> decomposition. Here the resonant plasma reactor<sup>15</sup> is used as the plasma system.

The laser light source is distributed-feed-back (DFB) QCL (LA1218, Hamamatsu) whose wavelength is about 6.1  $\mu\text{m}$  and peak power is 10 mW. The optical output power can be controlled by the pulse voltage applied to the laser diode and the pulse width. In this study, we use a pulse voltage of  $-10.65$  V and a pulse width of 120 ns. The constant bias voltage applied to the laser diode is  $-5$  V. The wavelength of this laser can be varied (within a relatively narrow range) by the control of its temperature with a peltier temperature controller. When the temperature is varied from  $-7.6$  to  $-3.4$   $^{\circ}\text{C}$ , the laser wavelength varies from 6.091 to 6.093  $\mu\text{m}$ . The laser beam is collimated by CaF<sub>2</sub> lenses to a diameter of 1.8 mm. The wavelength of QCL is calibrated based on NO<sub>2</sub> absorption lines obtained from HITRAN database.<sup>21,22</sup> The photo detector (i.e., infrared detector in Figure 4) is an InSb photoconductive device (P6606-320, Hamamatsu).

In Figure 4, a nanosecond-pulse generator, a waveform shaping circuit, a reference-voltage control circuit, and a 24 bit counter circuit constitute the ATTC circuit. Here a personal computer (PC) with a high-precision time measurement device measures the sequence time [i.e.,  $T_i = N(t + \Delta t_i)$  of Figure 2] with high accuracy. The number of laser shots used to evaluate each sequence time  $T$  is typically  $N = 273 \times 2^6 = 17472$ . The sequence time  $T$  is evaluated 60 times per second during the experiment.

The gas introduced to the reactor is a mixture of NO<sub>2</sub>, O<sub>2</sub>, and N<sub>2</sub>. The gas mixture ratio and the flow rate are controlled by mass flow controllers. The input gas used in study

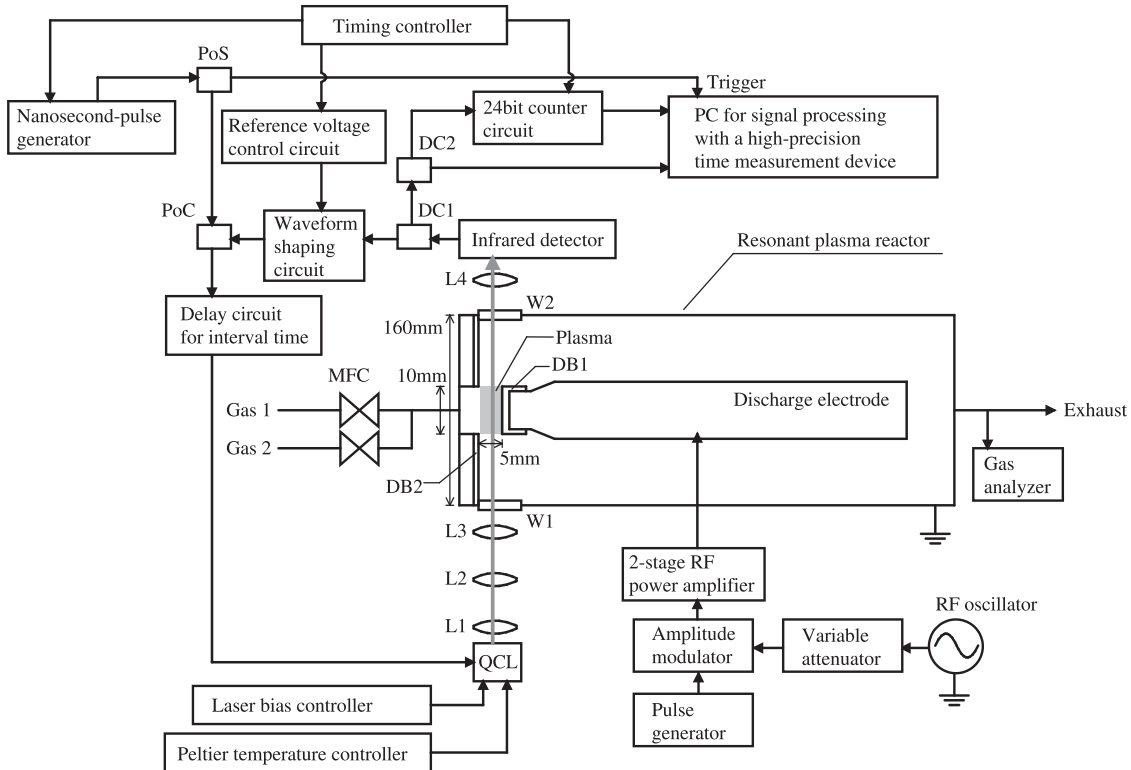


FIG. 4. Block diagram of the absorption spectroscopy measurement system with a resonant plasma reactor.<sup>15</sup> With this system, the NO<sub>2</sub> concentration is measured in the plasma system. The acronyms denote the following: PoS: power splitter, PoC: power combiner, DC1, DC2: directional couplers, L1-L4: CaF<sub>2</sub> lenses, W1, W2: CaF<sub>2</sub> optical windows, Gas 1: (N<sub>2</sub> 80%, O<sub>2</sub> 20%), Gas 2: (NO<sub>2</sub> 474 ppm, N<sub>2</sub> 99.95%), MFC: mass flow controller, and DB1, DB2: Al<sub>2</sub>O<sub>3</sub> dielectric barriers.



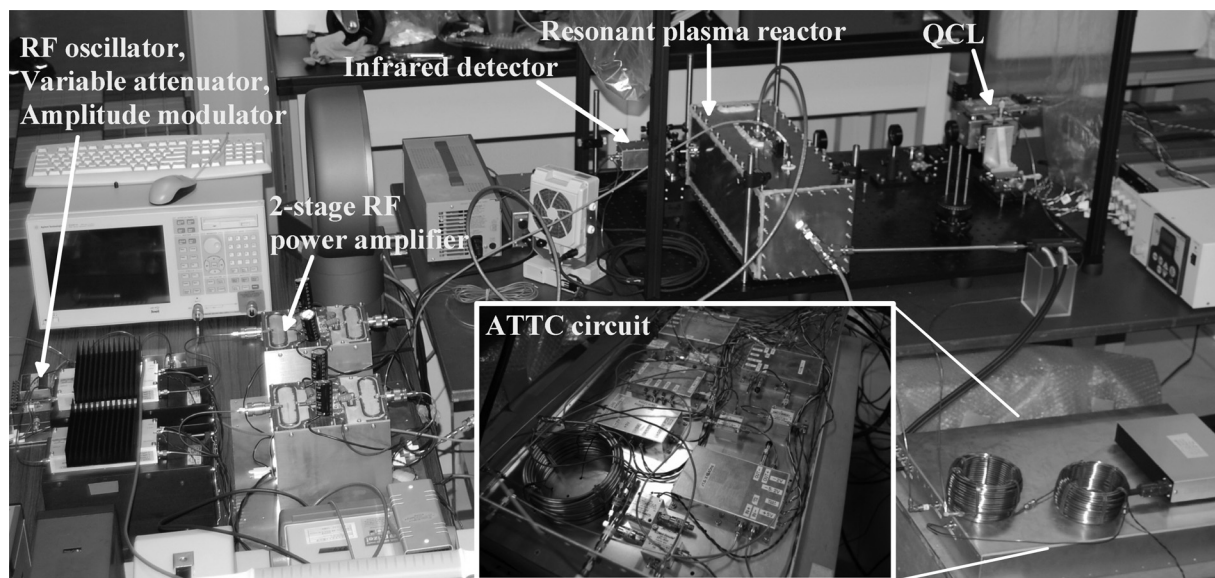


FIG. 5. Photograph of the experimental system. The inset shows the inside of the ATTC circuit box.

simulates a typical oxygen-rich diesel-engine exhaust gas and consists of  $\text{NO}_2$ ,  $\text{O}_2$ , and  $\text{N}_2$  with concentrations of 76 ppm, 17%, and 83%, respectively. Here we do not add  $\text{NO}$  into the input gas in order to focus on the concentration measurement of  $\text{NO}_2$ . The  $\text{NO}_2$  and  $\text{NO}$  concentrations in the gas treated by the resonant plasma reactor are measured by a gas analyzer (350XL, Testo) placed at the gas exit of the resonant plasma reactor. The gas analyzer is based on controlled-potential electrolysis.<sup>23</sup>

A schematic view of the resonant plasma reactor<sup>15</sup> is also given in Figure 4. The external metal frame of the reactor, which functions as the grounded electrode, has a shape of a rectangle box. Its outside dimensions are 160 mm in width, 160 mm in height, and 450 mm in length. The internal electrode is located at the center of the external metal frame and functions as the powered electrode. The length of the internal electrode is 320 mm, which was selected to be close to the half wavelength of RF wave. The resonance frequency of the system is 404 MHz. The power feeder is connected to the position near the center of the internal electrode. The exact impedance matching can be attained by the adjustment of the feeder position along the electrode.

One end of the internal electrode is covered with a dielectric barrier (DB1) made from alumina. This end of the electrode is placed near a wall of the external metal frame (i.e., grounded electrode), and the part of the grounded electrode facing the dielectric barrier of the internal electrode is also covered with an alumina dielectric barrier (DB2). Plasma is formed between these dielectric barriers. The electrode gap between the barriers is 5 mm. The center of the dielectric barrier on the grounded electrode has a small hole of a diameter of 10 mm, through which the gas is fed into the inside of the plasma reactor. The edge of the internal electrode is tapered to match the size of this hole. Plasma is generated near the gas inlet. Therefore the input gas flows through the plasma when a plasma is on.

In our pulse-modulated RF power supply, the waveform of input RF power is sinusoidal with the resonance

frequency, i.e., 404 MHz. The sinusoidal RF oscillation signal is modulated in time by an amplitude modulator, which is a field effect transistor (FET) switch module (ZYSWA-2-50DR, Mini-Circuits) and controlled by a pulse generator (33220A, Agilent technologies). The pulse modulated RF signal is then amplified by two-stage RF power amplifiers (ZHL-100W-50-S, Mini-Circuits; 0405-1000M, Microsemi). Therefore input RF power is modulated in time at the frequency of the pulse generator. We call this frequency the plasma modulation frequency. The instantaneous supplied power is 1350 W and the pulse width is 1.5  $\mu\text{s}$ . Figure 5 shows a photograph of the experimental system.

#### IV. EXPERIMENTAL RESULTS

The sequence time  $T_i$  [i.e.,  $T_i = N(t + \Delta t_i)$  in Figure 2] for absorption spectroscopy for  $\text{NO}_2$  was measured 60 times per second for the discharge experiment is plotted as a function of time  $\tau$  in Figure 6. In Figure 6, it is seen that plasma was on from  $\tau = 9$  min to 23 min. The simulated oxygen-rich exhaust gas ( $\text{N}_2$  83%,  $\text{O}_2$  17%) containing  $\text{NO}_2$  (76 ppm) started to flow into the plasma system at time  $\tau < 0$ . The gas

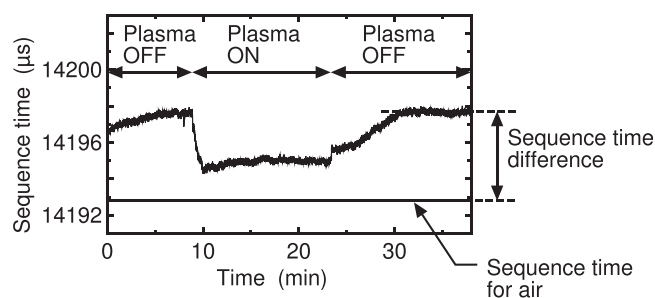


FIG. 6. Time variation of the sequence time  $T$ , reflecting the level of laser light absorption by  $\text{NO}_2$  gas in the plasma system when plasma was on and off. The sequence time  $T$  was evaluated 60 times per second. The QCL temperature was  $-6.8^\circ\text{C}$  (corresponding to the QCL wavelength of  $6.0913 \mu\text{m}$ ), the  $\text{NO}_2$  concentration of input gas was 76 ppm, and the gas flow rate was 1.2 l/min.

flow was continuous, and its rate was 1.2 l/min. When plasma was on, the instantaneous RF power was 1350 W, the pulse width was 1.5  $\mu$ s, and the plasma modulation frequency was 1200 Hz. The wavelength of QCL remained constant at 6.0913  $\mu$ m here for NO<sub>2</sub> detection. A higher sequence time  $T$  indicates larger absorption of laser light and therefore a higher concentration of NO<sub>2</sub> in the system.

It is seen that the sequence time  $T$  kept increasing slightly until about  $\tau = 5$  min, which indicates that the NO<sub>2</sub> concentration in the plasma system (without plasma) did not reach steady state before  $\tau = 5$  min. After plasma was turned on at  $\tau = 9$  min, the sequence time  $T$  dropped immediately. When the plasma was tuned off at  $\tau = 23$  min, the sequence time  $T$  increased gradually and returned to the original high value in about 8 min. In this way, we confirmed that the NO<sub>2</sub> concentration decreased in the presence of a plasma.

Although the data is not shown here, we also measured the sequence time in the same discharge system filled with dry air (i.e., sequence time for air). The representative value of the sequence time under specific gas conditions (i.e., with plasma being off in the discharge system filled with dry air or a simulated oxygen-rich exhaust gas, or with plasma being on in the discharge system filled with a simulated oxygen-rich exhaust gas) was obtained as the average of 512 sequence time values when the system was in steady state. The representative value of the sequence time for air is indicated in Figure 6. The difference between the obtained sequence time for an oxygen-rich exhaust gas (with or without plasma) and the sequence time for air is the “sequence time difference.”

The sequence time differences for the oxygen-rich exhaust gas without plasma (i.e., in the plasma-off conditions of Figure 6) were obtained in this manner for various laser wavelengths between 6.091 and 6.093  $\mu$ m. The laser wavelength was varied in this range by the control of its temperature from  $-7.6$  to  $-3.4$  °C at intervals of 0.2 °C. Figure 7(a) plots the sequence time difference as a function of the laser wavelengths. Typically it takes about 8 min to measure the entire set of sequence time differences plotted in this figure.

Since the NO<sub>2</sub> concentration of this gas was known to be 76 ppm, we compared the sequence time difference plotted in Figure 7(a) with the calculated absorption spectrum (i.e., absorbance as a function of the laser wavelength) given in Figure 11 obtained from HITRAN database. It is seen that there is excellent agreement in the shapes of the curves between Figure 7(a) and Figure 11. Comparing Figure 7(a) with Figure 11, we related the sequence time difference to the absorbance at each laser wavelength and plotted the relation in Figure 7(b) with empty circles. Figure 7(b) clearly shows the linear relation between the absorbance and the sequence time difference, which is consistent with the relation given in Eq. (1). The straight line in (b) is obtained from the least square fit of the calculated absorption spectrum of Figure 11 to the sequence time difference data of (a).

Using the relation given in Figure 7(b), we can now convert the sequence time difference to the absorbance. In Figure 8, we plotted the sequence time differences as functions of the laser wavelength under 4 different gas and plasma conditions. In (a), the conditions are the same as

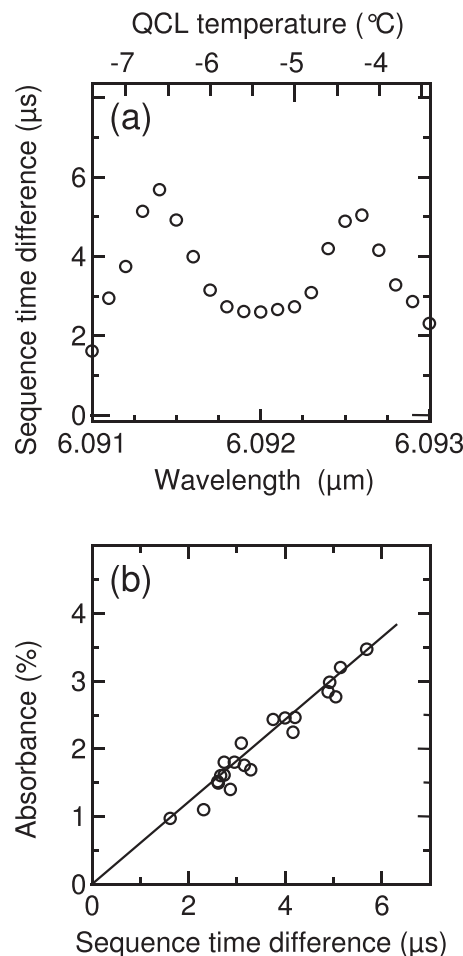


FIG. 7. (a) The sequence time differences measured in the plasma-off conditions of Figure 6 for various laser wavelengths. Since the NO<sub>2</sub> concentration in these conditions is known to be 76 ppm, the calculated absorption spectrum at this NO<sub>2</sub> concentration given in Figure 11 is compared with (a), and the relation between the absorbance and the sequence time difference is plotted by empty circles in (b). The straight line is obtained from the least square fit of the calculated absorption spectrum of Figure 11 to the sequence time difference data of (a).

those for the plasma-off period of Figure 6 (i.e., the conditions of Figure 7). In (b) and (c), the conditions are the same as those of the plasma-on period of Figure 6, except for the plasma modulation frequencies being 400 Hz and 800 Hz. In (d) all conditions are the same as those of the plasma-on period of Figure 6. Using the relation in Figure 7(b), we also indicate the corresponding absorbance on the left vertical axis of each graph. It is seen that when the plasma input power is higher, laser absorbance is lower, which means that less NO<sub>2</sub> is present in the plasma discharge region as the plasma decomposes NO<sub>2</sub>.

Noting that the NO<sub>2</sub> concentration is proportional to the absorbance, we fit the calculated absorption spectrum Figure 11 with variable magnitude to each graph of Figure 8. In (a), the fitted curve is the one that gives the proportional constant of Figure 7(b). From (b)–(d), we obtain the NO<sub>2</sub> concentration of each case by comparing the magnitude of the fitted absorption spectrum with that in (a). The obtained NO<sub>2</sub> concentrations for (b)–(d) are 38 ppm, 30 ppm, and 25 ppm, respectively.

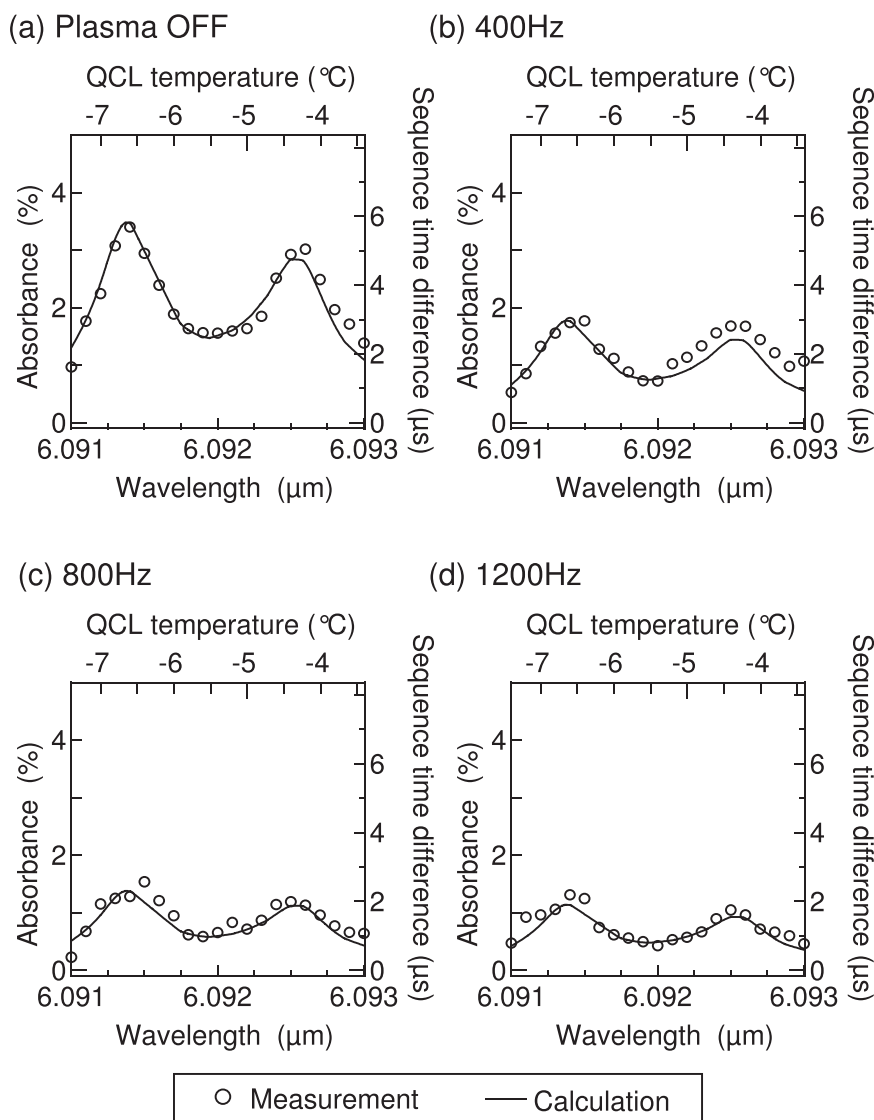


FIG. 8.  $\text{NO}_2$  absorption spectra at various plasma modulation frequencies; (a) plasma OFF, (b) 400 Hz, (c) 800 Hz, and (d) 1200 Hz. The gas flow rate is 1.2 l/min. The  $\text{NO}_2$  concentration without plasma [i.e., in (a)] is 76 ppm.

Figure 9 shows the  $\text{NO}_2$  concentration as functions of the plasma modulation frequency for three different flow rates of 1.2, 2.4, and 4.8 l/min. Other plasma conditions are the same as those for Figure 8. Here the plasma modulation frequency being zero means that no voltage is applied to the electrode, i.e., no plasma is present in the plasma system. The corresponding time-averaged power supplied to the plasma system (i.e., average supplied power) is also indicated in the upper horizontal axis, based on the instantaneous RF power of 1350 W. The  $\text{NO}_2$  concentrations at the flow rate of Figure 8 are given by filled circles in Figure 9. It is seen that more  $\text{NO}_2$  is decomposed by a plasma with higher input power. It is also seen that  $\text{NO}_2$  may be decomposed less by the plasma if the flow rate is higher. This is because, at a higher flow rate, the residence time of gas in the plasma region is shorter.

The  $\text{NO}$  and  $\text{NO}_2$  concentrations at the gas outlet of the plasma reactor were measured by a gas analyzer. Figure 10 compares the  $\text{NO}_2$  concentrations around the plasma with the  $\text{NO}_2$  and  $\text{NO}$  concentrations at the gas outlet of the plasma reactor as functions of the plasma modulation frequency. The curve (a) represents the  $\text{NO}_2$  concentration at the gas inlet (where the plasma was generated), which is

shown in Figure 9, whereas the curves (b) and (c) represent the  $\text{NO}_2$  and  $\text{NO}$  concentrations at the gas outlet. The gas flow rate was 1.2 l/min. The  $\text{NO}_2$  concentration at the gas inlet decreases with the plasma modulation frequency. However, the  $\text{NO}_2$  concentration at the gas outlet increases with the plasma modulation frequency and can be higher than that of the input gas when the modulation frequency is sufficiently high. In this system no  $\text{NO}$  was detected at the gas outlet.

## V. DISCUSSION ON REACTIONS OF $\text{NO}_x$ IN THE PLASMA REACTOR

### A. Gas expansion by discharge heating

In Sec. IV, we observed that the  $\text{NO}_2$  concentration at the gas inlet decreased when plasma was generated in the electrode gap near the gas inlet. This, however, may not mean that  $\text{NO}_2$  was decomposed by the plasma since the  $\text{NO}_2$  concentration can also decrease without decomposition if the gas volume expands by discharge heating. In this subsection, we estimate a possible increase of the gas volume by discharge heating.



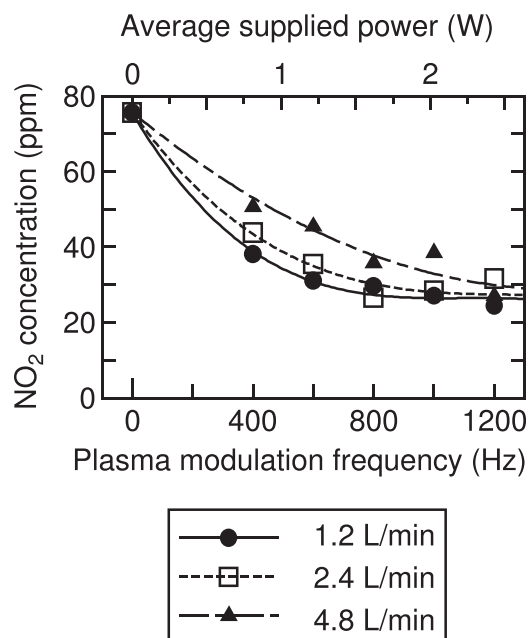


FIG. 9. Dependence of NO<sub>2</sub> concentrations on the plasma modulation frequency (and the corresponding average supplied power for plasma generation in the plasma system) for three different flow rates of 1.2, 2.4, and 4.8 l/min. Other plasma conditions are the same as those of Figures 6 and 8.

The experimental conditions for Figure 10 are summarized in Table I. We also assume that the heat capacity of the sample gas is the same as that of nitrogen, i.e., 29 J/mol K. From the data of Table I, we estimate the typical gas residence time is 20 ms and, during this residence time, the total power supplied to the system is 2.4 W. If all the power were used to increase the temperature, the temperature would

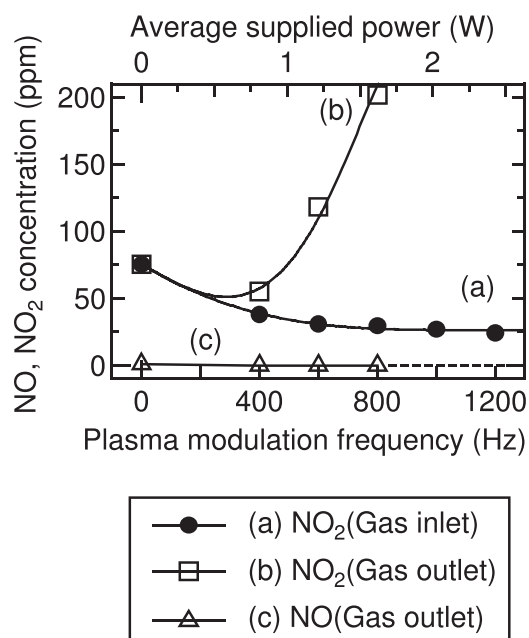


FIG. 10. Dependence of NO<sub>2</sub> and NO concentrations at the gas inlet and outlet of the plasma system on the plasma modulation frequency. (a) The NO<sub>2</sub> concentration at the gas inlet (where plasma is generated) measured by QCL absorption spectroscopy. The NO<sub>2</sub> (b) and NO (c) concentrations at the gas outlet measured by the controlled-potential electrolysis. The gas flow rate is 1.2 l/min.

TABLE I. Experimental conditions.

NO <sub>2</sub> concentration	76 ppm
Gas flow rate	1.2 l/min = 20 cm <sup>3</sup> /s
Volume of plasma	0.39 cm <sup>3</sup>
Pulse width	1.5 μs
Plasma modulation frequency	1200 Hz
Instantaneous RF power	1350 W
Average supplied power	2.43 W

increase by 100 °C. With the initial gas temperature being 20 °C, the volume of heated gas would not be any larger than about 130% of the initial gas volume, which means that the maximum possible decrease of the concentration by thermal gas expansion would be only about 30%. Since Figure 10 shows that the NO<sub>2</sub> concentration decreases nearly 70%, we conclude that thermal gas expansion alone cannot account for the decrease in the NO<sub>2</sub> concentration observed here and therefore NO<sub>2</sub> is indeed decomposed by the plasma.

## B. Gas-phase chemical reactions associated with NO<sub>2</sub> decomposition

In this subsection, we list gas-phase chemical reactions with relatively high rate constants associated with NO<sub>2</sub> decomposition in order to access possible reaction paths that may take place in the plasma reactor in our experiments.

In earlier studies, it is known that chemically reactive atomic species such as N and O are generated within about 10 ms after the initiation of air discharge.<sup>24</sup> Collisions with such atomic species as well as electrons can decompose NO<sub>2</sub> through, for example, the following reactions:<sup>25–27</sup>

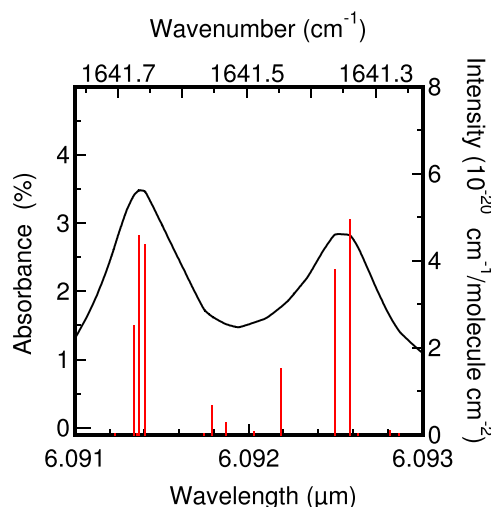
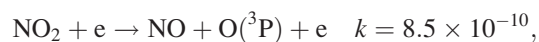
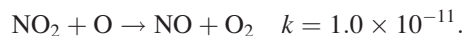
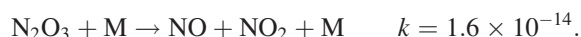
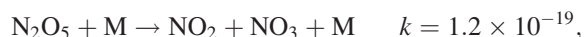


FIG. 11. NO<sub>2</sub> absorption spectrum calculated from HITRAN 2004 database<sup>21,22</sup> for a NO<sub>2</sub> concentration of 76 ppm, a total gas pressure of 1 atm, a temperature of 296 K, and an optical path length of 16 cm.



Here the units of the rate constant  $k$  are  $\text{cm}^3 \text{mol}^{-1} \text{s}^{-1}$ . These reactions generate NO, NO<sub>3</sub>, and N<sub>2</sub>O and reduce the NO<sub>2</sub> concentration at the plasma discharge.

However, as these species travel through the plasma reactor together with other gas species, they can be further converted to other (typically high-order) NO<sub>x</sub> through the following slower chemical reactions:<sup>27</sup>



Here M indicates a gas molecule of air (N<sub>2</sub> and O<sub>2</sub>) that has the highest concentration. In air discharge, the ozone concentration is also high, so the reactions above occur at high rates although some of the rate constants are relatively low. These reaction equations suggest that, after forming various intermediate species such as N<sub>2</sub>O<sub>3</sub>, the initial input gas NO<sub>2</sub> is likely to return to NO<sub>2</sub> eventually. Some earlier studies<sup>24</sup> suggest NO<sub>3</sub> and N<sub>2</sub>O. N<sub>2</sub>O<sub>5</sub> also remain for a long period after the termination of plasma discharge. In this study, we did not measure the concentrations of these chemical species, and such measurements are a subject of future study. Especially N<sub>2</sub>O is known as a green-house gas and should be treated before being emitted to atmosphere.

## VI. CONCLUSIONS

In this study, we have measured the NO<sub>2</sub> concentration in a small plasma of a NO<sub>x</sub> treatment reactor by QCL absorption spectroscopy with the ATTC technique.<sup>20</sup> The high sensitivity of the spectroscopy system allows the measurement of a molecular concentration in a gas with a relatively short optical path length.

If the gaseous species of interest has a low concentration or the optical path for laser absorption is short, absorption spectroscopy is required to detect small attenuation of laser light that passes through the gas. This may be achieved by detecting the amplitude of laser light at high resolution. However, if the difference in amplitude between the attenuated and unattenuated laser beams is small, the majority of digital data obtained from an analog-to-digital (A/D) converter representing the laser beam amplitude is not used effectively in the evaluation of difference in laser beam amplitude.

In contrast, in the ATTC technique, the rise times of laser pulse signals are added over a large number of pulses of the same kind, and therefore the average rise time is evaluated accurately with reduced statistical noises. Since the rise time of

a pulse signal is closely related to its amplitude, the difference in rise time between the attenuated and unattenuated laser pulse signals can be converted back to the difference in amplitude between those signals. The advantage of the ATTC technique is that it can add and average analogue signals with statistical noises (i.e., rise times of laser pulse signals in the present case) without digitizing the original signals by an A/D converter.

In this paper, after a brief description of the ATTC technique, a system for QCL absorption spectroscopy is presented. The signal processing for the spectroscopy is based on the ATTC technique and the system is set up as a diagnostic tool for a plasma reactor for NO<sub>x</sub> treatment. The plasma reactor is designed to convert NO in the input gas to NO<sub>2</sub>.<sup>15</sup> The plasma is generated between the electrodes whose gap length is 5 mm, and the lateral size of the powered electrode is about 1 cm. The optical path for absorption spectroscopy, which traverses the electrode gap, is 16 cm.

Using the absorption spectroscopy system, we have measured the concentration of NO<sub>2</sub> in the discharge region of the plasma reactor with a simulated exhaust gas (N<sub>2</sub> 83%, O<sub>2</sub> 17% with a 76 ppm of NO<sub>2</sub>) as the input gas. It has been found that, although the reactor is designed to decompose NO to form NO<sub>2</sub>, NO<sub>2</sub> is also decomposed by the plasma. However NO<sub>2</sub> is formed again through a series of gas-phase reactions by the time the gas exits the reactor. The observation is consistent with that of an earlier study on NO decomposition by the same type of a plasma reactor,<sup>15</sup> in which a high concentration of NO<sub>2</sub> was observed at the exit of the reactor.

## ACKNOWLEDGMENTS

This study was carried out with the support of the Laboratory for Osaka University-Mitsui Engineering and Shipbuilding Joint Research Chair (Plasma Technology and Engineering).

## APPENDIX A: NO<sub>2</sub> ABSORPTION SPECTRUM

Absorption spectra in Figure 8 are determined theoretically in the following manner. Absorption line spectrum of NO<sub>2</sub> for vibrational and rotational levels with their pressure broadening is taken from HITRAN 2004 database.<sup>21,22</sup> Superposition of Lorentzian functions for all spectral lines obtained from the database is given in Figure 11 for a NO<sub>2</sub> concentration of 76 ppm, a total pressure of 1 atm, a temperature of 296 K, and an optical path length of 16 cm. The position and height of each spectral line are indicated by the vertical bar. Energy levels of main spectral lines shown here are summarized in Table II.

TABLE II. Energy levels of main NO<sub>2</sub> spectral lines shown in Figure 11.

Center wavenumber (cm <sup>-1</sup> )	Upper level (ν <sub>1</sub> ν <sub>2</sub> ν <sub>3</sub> )-(J' Ka' Kc')	Lower level (ν <sub>1</sub> ν <sub>2</sub> ν <sub>3</sub> )-(J'' Ka'' Kc'')
1641.340	(0 0 1)-(33 0 33)	(0 0 0)-(32 0 32)
1641.364	(0 0 1)-(34 2 33)	(0 0 0)-(33 2 32)
1641.657	(0 0 1)-(34 1 34)	(0 0 0)-(33 1 33)
1641.667	(0 0 1)-(33 1 32)	(0 0 0)-(32 1 31)
1641.676	(0 0 1)-(36 3 34)	(0 0 0)-(35 3 33)

TABLE III. Comparison of detectable minimum values of NO<sub>2</sub> concentrations by various QCL absorption spectroscopy used in Refs. 28–30 and this study (i.e., the ATTC technique).<sup>20</sup>

Reference	Gas	Length of gas cell (cm)	Number of path	Optical path length (cm)	Detectable minimum concentration (ppm)	Detectable minimum concentration (ppm at 10 cm)	Ratio of absorbances	Detectable minimum concentration for NO <sub>2</sub> equivalent (ppm at 10 cm)
28	NO <sub>2</sub>	12.5	9	112.5	0.47	5.27	1	5.27
29	NO	2.54	9	22.86	67	153.16	5.65	27.1
30	NO	...	...	10000	0.016	16	5.65	2.83
ATTC	NO <sub>2</sub>	10	1	10	1.7	1.7	1	1.7

## APPENDIX B: COMPARISON BETWEEN CONVENTIONAL LASER ABSORPTION SPECTROSCOPY AND THAT WITH THE ATTC TECHNIQUE

The sensitivity of laser absorption spectroscopy may be represented by the smallest detectable attenuation of a laser light that passes through the plasma and gas. In ordinary absorption spectroscopy, the detectable minimum value for attenuation is limited by the bit size of the A/D converter used for the amplitude measurement of photo detector signals. With a 16 bit A/D converter, the theoretical limit for minimum attenuation value in such a measurement is  $2^{-16} = 1/65536$  of the total amplitude of the photo-detector signal. In laser absorption spectroscopy with the ATTC technique, on the other hand, the decrease of laser light amplitude due to optical absorption is converted to the “sequence time difference,” as discussed in Sec. II. Since the sequence time difference can be magnified by the increase of the number of laser shots  $N$  for laser absorption measurement, it can be obtained with an ordinary time counter.

Indeed we evaluated the concentrations of NO<sub>2</sub> gas samples by directly measuring the photo-detector signal amplitudes in laser absorption spectroscopy as well as measuring the sequence time differences in the ATTC based laser absorption spectroscopy.<sup>20</sup> For these experiments, we used NO<sub>2</sub> gas samples with various concentrations contained in gas cells whose optical paths are 10 cm in length. In the case of direct amplitude measurement, the minimum NO<sub>2</sub> concentration that we were able to obtain was about 100 ppm whereas the minimum NO<sub>2</sub> concentration that we obtained by the ATTC based laser absorption spectroscopy was 1.7 ppm. In other words, we demonstrated 50 times improvement in sensitivity by introducing the ATTC technique.

Several highly sensitive methods for QCL absorption spectroscopy for NO or NO<sub>2</sub> were proposed in the earlier studies of Refs. 28–30. In these studies, multiple reflection optical systems are used to increase the optical path lengths and the photo-detector amplitudes were measured by lock-in amplifiers or high resolution A/D converters. Table III summarizes the results of these studies as well as our results based on the ATTC technique. In Refs. 29 and 30, NO concentrations, rather than NO<sub>2</sub> concentrations, were measured. Since the NO<sub>2</sub> absorbance is 5.65 times higher than the NO absorbance, this ratio (denoted as “Ratio of absorbance”) was used to evaluate the detectable minimum values for

possible NO<sub>2</sub> concentrations by the methods of Refs. 29 and 30 (which are listed under the “Detectable minimum concentration of NO<sub>2</sub> equivalent” in Table III).

- <sup>1</sup>P. Granger, C. Dujardin, J.-F. Paul, and G. Leclercq, *J. Mol. Catal. A: Chem.* **228**, 241 (2005).
- <sup>2</sup>E. C. Corbos, M. Haneda, X. Courtois, P. Marecot, D. Duprez, and H. Hamada, *Appl. Catal., A* **365**, 187 (2009).
- <sup>3</sup>M. Ruszak, M. Inger, S. Witkowski, M. Wilk, A. Kotarba, and Z. Sojka, *Catal. Lett.* **126**, 72 (2008).
- <sup>4</sup>M. Koebel, M. Elsener, and M. Kleemann, *Catal. Today* **59**, 335 (2000).
- <sup>5</sup>R. van Helden, R. Verbeek, F. Willems, and R. van der Welle, “Optimization of urea SCR deNO<sub>x</sub> systems for HD diesel engines,” SAE Technical Paper No. 2004-01-0154, 2004.
- <sup>6</sup>S. Yoon, A. G. Panov, R. G. Tonkyn, A. C. Ebeling, S. E. Barlow, and M. L. Balmer, *Catal. Today* **72**, 243 (2002).
- <sup>7</sup>T. Yamamoto, M. Okubo, T. Nagaoka, and K. Hayakawa, *IEEE Trans. Ind. Appl.* **38**, 1168 (2002).
- <sup>8</sup>T. Hammer, *Plasma Sources Sci. Technol.* **11**, A196 (2002).
- <sup>9</sup>A. Fridman, *Plasma Chemistry* (Cambridge, New York, 2008), p. 817.
- <sup>10</sup>B. M. Penetrante, R. M. Brusasco, B. T. Merritt, and G. E. Vogtlin, *Pure Appl. Chem.* **71**, 1829 (1999).
- <sup>11</sup>J. S. Chang, *Plasma Sources Sci. Technol.* **17**, 045004 (2008).
- <sup>12</sup>L. Civitano, *Non-Thermal Plasma Techniques for Pollution Control Part B*, edited by B. M. Penetrante and S. E. Schultheis (Springer, Berlin, 1993), p. 103.
- <sup>13</sup>M. B. Chang, M. J. Kushner, and M. J. Rood, *Environ. Sci. Technol.* **26**, 777 (1992).
- <sup>14</sup>U. Kogelschatz, *Plasma Chem. Plasma Process.* **23**, 1 (2003).
- <sup>15</sup>T. Yumii, T. Yoshida, K. Doi, N. Kimura, and S. Hamaguchi, *J. Phys. D* **46**, 135202 (2013).
- <sup>16</sup>J. Faist, F. Capasso, D. L. Sivco, C. Sirtori, A. L. Hutchinson, and A. Y. Cho, *Science* **264**, 553 (1994).
- <sup>17</sup>R. F. Curl, F. Capasso, C. Gmachl, A. A. Kosterev, B. McManus, R. Lewicki, M. Pusharsky, G. Wysocki, and F. K. Tittel, *Chem. Phys. Lett.* **487**, 1 (2010).
- <sup>18</sup>H. Page, C. Becker, A. Robertson, G. Glastre, V. Ortiz, and C. Sirtori, *Appl. Phys. Lett.* **78**, 3529 (2001).
- <sup>19</sup>M. Razeghi, *IEEE J. Sel. Top. Quantum Electron.* **15**, 941 (2009).
- <sup>20</sup>T. Yumii and N. Kimura, *J. Plasma Fusion Res.* **88**, 211 (2012) (in Japanese).
- <sup>21</sup>L. S. Rothman, D. Jacquemart, A. Barbe, D. C. Benner, M. Birk, L. R. Brown, M. R. Carleer, C. Chackerian, Jr., K. Chance, L. H. Coudert, V. Dana, V. M. Devi, J.-M. Flaud, R. R. Gamache, A. Goldman, J.-M. Hartmann, K. W. Jucks, A. G. Maki, J.-Y. Mandin, S. T. Massie, J. Orphal, A. Perrin, C. P. Rinsland, M. A. H. Smith, J. Tennyson, R. N. Tolchenov, R. A. Toth, J. V. Auwera, P. Varanasi, and G. Wagner, *J. Quant. Spectrosc. Radiat. Transfer* **96**, 139 (2005).
- <sup>22</sup>P. W. Morrison, Jr. and O. Taweechokesupin, *J. Electrochem. Soc.* **145**, 3212 (1998).
- <sup>23</sup>D. T. Sawyer and J. L. Roberts, Jr., *Experimental Electrochemistry for Chemists* (John Wiley & Sons, New York, 1974), p. 329.
- <sup>24</sup>B. Eliasson and U. Kogelschatz, *IEEE Trans. Plasma Sci.* **19**, 1063 (1991).
- <sup>25</sup>T. de los Arcos, M. Castillo, C. Domingo, V. J. Herrero, M. M. Sanz, and I. Tanarro, *J. Phys. Chem. A* **104**, 8183 (2000).
- <sup>26</sup>S. Teodoru, Y. Kusano, and A. Bogaerts, *Plasma Process. Polym.* **9**, 652 (2012).

- <sup>27</sup>J. A. Manion, R. E. Huie, R. D. Levin, D. R. Burgess, Jr., V. L. Orkin, W. Tsang, W. S. McGivern, J. W. Hudgens, V. D. Knyazev, D. B. Atkinson, E. Chai, A. M. Tereza, C.-Y. Lin, T. C. Allison, W. G. Mallard, F. Westley, J. T. Herron, R. F. Hampson, and D. H. Frizzell, NIST Chemical Kinetics Database, NIST Standard Reference Database 17, Version 7.0 (Web Version), Release 1.4.3, Data version 2008.12, National Institute of Standards and Technology, Gaithersburg, Maryland, 20899-8320. URL: <http://kinetics.nist.gov/>.
- <sup>28</sup>A. Karpf and G. N. Rao, *Appl. Opt.* **48**, 408 (2009).
- <sup>29</sup>S. Wehe, D. Sonnenfroh, M. Allen, C. Gmachl, and F. Capasso, "Measurements of trace pollutants in combustion flows using room-temperature, mid-ir quantum cascade lasers," AIAA Paper 2002-0824, 2002.
- <sup>30</sup>L. Menzel, A. A. Kosterev, R. F. Curl, F. K. Tittel, C. Gmachl, F. Capasso, D. L. Sivco, J. N. Baillargeon, A. L. Hutchinson, A. Y. Cho, and W. Urban, *Appl. Phys. B* **72**, 859 (2001).